Composite Structures 131 (2015) 312–324

Contents lists available at ScienceDirect

Composite Structures

journal homepage: www.elsevier.com/locate/compstruct

Model for piezoelectric/ferroelectric composites polarized with interdigitated electrodes

Ahmad Eduardo Guennam [a,*], Bibiana M. Luccioni [a,b]

[a] Structures Institute, National University of Tucuman, Avenida Roca 1800, SM de Tucuman, Argentina
[b] CONICET, Avenida Rivadavia 1917, Buenos Aires, Argentina

ARTICLE INFO

Article history:
Available online 6 May 2015

Keywords:
Piezoelectric composite
Interdigitated electrode
Nonlinear
Repolarization
Hysteresis
Cutting-planes

ABSTRACT

A piezoelectric composite homogenization model (PCHM) is presented in this article. A systematic method for predicting the composite macroscopic history-dependent electromechanical response is developed and particularized for piezoelectric fiber composites polarized with interdigitated electrodes. As other composite models, the proposed PCHM requires appropriate constitutive equations describing each pure constituent namely, fiber and matrix. In this work, dielectric matrix is modeled as electromechanically linear while an existing non-linear phenomenological model is used for the fibers. Additionally, a cutting-plane algorithm is developed and implemented to integrate the fibers constitutive equation. The proposed PCHM is implemented in a previously developed ABAQUS/UEL piezoelectric shell.

To evaluate the proposed model, a representative elementary volume (REV) is analyzed with a finite element (FE) model using an ABAQUS/UEL piezoelectric brick and the same material models for each constituent of the composite. Practical examples are addressed with both, FE/REV and the proposed PCHM. Electromechanical responses predicted with both approaches are in good agreement. Numerical results illustrate the ability of the proposed PCHM to capture important aspects of piezoelectric devices such as quasi-linear range, as well as both, pressure and electric-field driven depolarization. Finally, a brief convergence analysis is performed indicating an encouraging computational performance of the proposed PCHM.

1. Introduction

Modern civilization evolution relies, to some extent, on the development of complex and efficient systems. Accordingly, several branches of science and technology are focused on developing systems with the ability of assessing a given situation and responding in a suitable manner. This functionality confers outstanding ability to fulfill the task or function for which they were designed. Despite the wide application range and diversity of the aforementioned kind of systems, some common desired features are devised e.g. optimum functionality, adaptation ability and integrated design [1]. A technological area deeply involved in active systems development is that one concerning active structures. The performance level achieved by them is very promising for numerous practical applications. The potential of these systems is reflected in the number of research papers focused on the subject published during the last decade [2–6].

Piezoelectric composites are attractive active materials. They could be used for constructing smart devices with imminent technological applications. Because of the great potential of piezoelectric composite materials in active structures and other micro-electromechanical systems, accurate material models capable of predicting their properties and response are of great interest. In structural applications, engineers and designers are generally focused on devices overall response. In those cases, the main objective of the modeling is the prediction of macroscopic material response avoiding an explicit constituent discretization. This topic has recently become the subject of intensive study. In this context, the development of reliable and efficient design and modeling tools is of main interest.

2. Literature review

Reliable and effective calculation tools for the effective properties of piezoelectric composites are highly desirable for the design of structural systems using this kind of materials. According to [7], first Maxwell [8] and Wagner [9] later, did, maybe, the initial

* Corresponding author.
E-mail address: eguennam@herrera.unt.edu.ar (A.E. Guennam).

http://dx.doi.org/10.1016/j.compstruct.2015.04.014
0263-8223/

attempts to theoretically predict the dependence of dielectric properties of a composite from its ceramic volume fraction. Five decades later, Buesson and Klinsberg [10] derived equations for the dielectric constants using series/parallel models. Subsequent models based on the aforementioned research were developed for piezoelectric composites. Earlier investigations were focused on deriving the properties of piezoelectric composites consisting of spherical inclusions immersed in a polymeric matrix. Later, these approaches were extended to consider piezoelectric fibers reinforced composites and others models have been proposed.

Numerous research works dealing with different approaches for the evaluation of the effective piezoelectric composite properties can be found in the specialized literature. Following [11], typical methods for the determination of the macroscopic properties of inhomogeneous media could be classified into three categories, namely effective medium theories, theoretical bounding methods and computational simulations. The former theories include the Eshelby, Mori–Tanaka [12] methods, self-consistent scheme [13,14], and other mean-field models [15]. The theoretical bounding methods consist of the Hashin–Shtrikman [16] lower and upper bounds as well as other higher-order bounds. Finally, the computationally intensive models typically use finite element or boundary element methods to calculate the response of a representative volume element of piezoelectric composites [15,17–19].

Investigations developed by Wang [20], Dunn and Taya [21], Chen [22] and Shodja et al. [23] extend the Eshelby classical solution for an infinite medium with ellipsoidal inclusions, in order to include the piezoelectric aspect. These approaches do not take into account the interactions between inclusions. The model presented by Odegard [24] is based on the self-consistent Mori–Tanaka method and the extensions proposed by Dvorak and Srinivas [25]. Other models were proposed for the analysis of history dependent non-linear effects in piezoelectric composite materials. The model proposed by Tan and Tong [26] uses uniform field model to capture the response to moderate and monotonic electric fields. Aboudi [27,28] uses a homogenization micro-mechanic based model for the study of the hysteretic response of a composite reinforced with ferroelectric fiber with periodic structure. Muliana [29] presents a simplified micro-electromechanical model averaging the field variables inside the volume. The model includes the hysteretic phenomena, repolarization of the fibers and the viscoelastic matrix effects. For this purpose, the model considers the electric field as a constant parameter, expressing the non-linear electromechanic coupling relations in terms of mechanic stress and electric field components.

Computational intensive approaches analyze the composite response identifying a representative elementary volume (REV), typically denoted as unit cell. The unit cell is identified in such a way that it exhibits the more relevant properties of the composite microstructure. Then, it is explicitly modeled and, by imposing suitable boundary conditions, the effective electromechanical properties are calculated. The electric field pattern and the ability to explode different coupling modes of piezo-composites are closely related to electrodes configuration. Bent and Hagood [15] propose a material model for piezoelectric composite laminates polarized with interdigitated electrodes. The model uses the uniform field method to obtain the effective material properties. The investigation includes comparisons with a finite element model for different constituent material properties, volume relations and electrodes geometric aspects. Based on this last model, Luccioni [30] proposes a formal, systematic approach in order to make series and parallel combinations of mechanical non-linear models. Martinez and Artemev [18] present a computationally intensive analysis of actuators and sensors constructed with piezoelectric laminates polarized with interdigitated electrodes. The analysis considers the presence of damaged fibers and the depolarization near the damaged zones. The authors present a quantification of the performance degradation associated with the fiber damage, reporting degradation levels up to 10%. Jayendiran and Arockiarajan [31] and Lin and Muliana [32] present simplified microelectromechanical models and physical tests for overall hysteretic response of active, 1–3 and 0–3 piezocomposites samples polarized with plate-type electrodes.

Interdigitated electrode pattern allows to exploit the maximum piezoelectric coupling [33] when in-plane actuation is needed, mainly in thin walled structures. Therefore, a numerical material model for composites reinforced with piezoelectric fibers polarized with interdigitated electrodes is presented in this paper. Based on the general composite materials mechanical model proposed by Luccioni [30], a systematic method for predicting the history dependent electromechanical material behavior and properties is developed in this work, emphasizing its relatively easy implementation and inclusion in a variety of general purpose finite element codes within an incremental analysis framework.

3. Proposed piezoelectric composite material model

As stated in the preceding section, the proposed piezoelectric composite homogenization model (PCHM) combines and extends existing approaches [15,30] introducing the electromechanical fields that take place in the considered piezoelectric composites in order to obtain their macroscopic properties, state and internal variables.

As other composite models, the proposed PCHM requires appropriate constitutive equations (CEs) of each pure constituents namely, fiber and matrix. A variety of constitutive models for the piezoelectric fibers, either linear or non-linear, can be included in the proposed model structure. In the context of this paper, the phenomenological ferroelectric model proposed by Huber and Fleck [34] is implemented along with a cutting plane algorithm, proposed in this work, to integrate the CE. This phenomenological model performs quite well for uni-axial loading states, which is consistent with fibers immersed in a soft matrix and far enough from electrodes zones. It exhibits good balance between implementation effort and ability to capture most of the main features of ferroelectric materials, e.g. independent evolution of both, strain and polarization states, as well as electric field and stress driven depolarization. The proposed homogenization model admits, certainly, the possibility of including other, more complex and reliable models.

Since various ideas and models from previous works are employed, it is convenient to state that the main contribution of this article is the combination of existing models, extending one of them to be able to handle electromechanical fields and the numerical implementation in the general purpose finite element package ABAQUS [35]. Fig. 1 underlines the fundamental models, ideas and their interrelations contributing to the proposed model.

3.1. Composite idealized representation

A piezoelectric composite lamina has the appearance depicted in Fig. 2. The lamina response is the result of various phenomena and processes taking place at different scales inside it. These scales definition are rather arbitrary and conveniently adopted for the analysis being performed. The fibers behavior could be analyzed with an approach characterized by a length scale called micro-electrom echanical. The combination of fibers with a polymeric matrix forms the lamina whose analysis corresponds to the meso-scale. Finally, the macro-electromechanical scale is related to the behavior of piezoelectric laminate at structural level, when disposed as actuator or sensor.

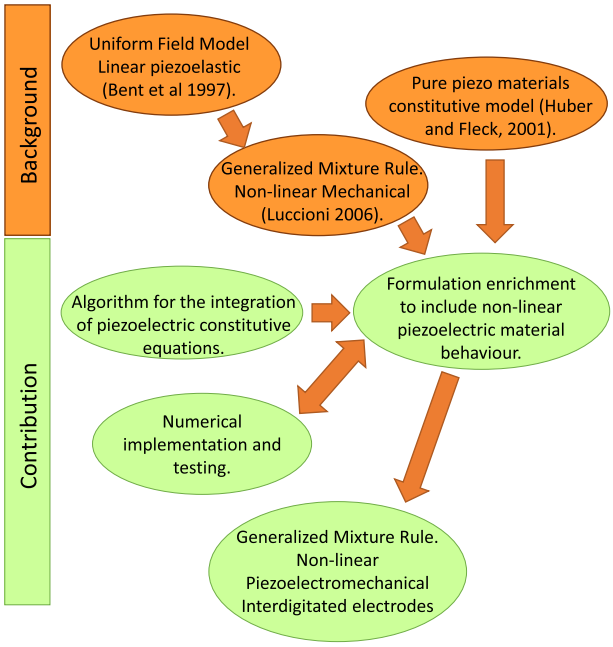

Fig. 1. Previous work, background and "this paper" contribution scheme.

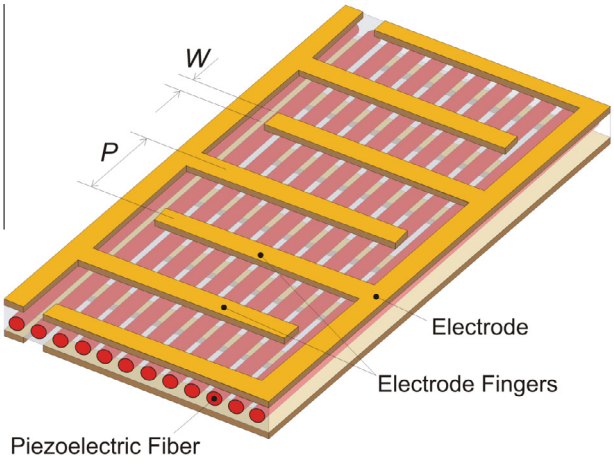

Fig. 2. Single lamina of piezoelectric composite polarized with interdigitated electrodes.

In this work, the matrix behavior is assumed linear-elastic while the fiber material response is described with the classical constitutive equations for piezoelectric media, expressed, in indicial notation, by

$$\sigma_{ij} = C^E_{ijkl}\left(\epsilon_{kl} - \epsilon^r_{kl}\right) - e_{kij}E_k \tag{1}$$

$$D_i - P^r_i = e_{ikl}\left(\epsilon_{kl} - \epsilon^r_{kl}\right) + \chi^\epsilon_{ik}E_k \tag{2}$$

where the fourth rank tensor C^E_{ijkl} is the mechanical stiffness tensor at constant electric field, e_{kij} is the piezoelectric tensor and χ^ϵ_{ik} is the dielectric module measured at constant strain. The internal state variables ϵ^r_{kl} and P^r_i are the remanent strain and polarization respectively. σ_{ij} is the stress tensor, ϵ_{kl} is the strain tensor, D_i is the electric displacement vector and E_k the electric field vector.

Both, C^E_{ijkl} and χ^ϵ_{ik} are assumed constants. However, piezoelectric tensor is assumed to be function of P^r_i, with the following simple functional relation:

$$e_{kij} = \frac{P^r}{P_0}\left[e_{33}n_k n_i n_j + e_{31}n_k\alpha_{ij} + \frac{1}{2}e_{15}\left(n_i\alpha_{jk} - n_j\alpha_{ik}\right)\right] \tag{3}$$

where,

$$P^r = \sqrt{P^r_i P^r_i} \tag{4}$$

$$n_i = \frac{P^r_i}{P^r} \tag{5}$$

$$\alpha_{ij} = \delta_{ij} - n_i n_j \tag{6}$$

The meso-electromechanic scale approach allows modeling the composite behavior based on the properties of each phase and on geometric aspects namely volume fractions, electrode spacing and electrode width.

Based on electrodes pattern, fiber arrangement and geometry of the considered piezoelectric composite, a RVE or unit cell is identified. The model assumes that the unit cell could be constructed in three stages (A, B and C). The three stages are represented in Fig. 3 where the successive composition is presented. In each stage, two material phases are distinguished and combined to give rise to a homogeneous equivalent material. In the next stage, this homogeneous material is combined with a new portion of polymeric matrix. For clarity, the fiber is represented in black and the matrix in white. Different gray shades are used for the resulting partial material as the successive combinations take place. Each composition stage introduces a particular aspect which could be identified in the composite behavior. The matrix portion parallel to the fiber introduces stress and strain distribution effects in both longitudinal and transversal directions, as function of constituent disposition and volumetric fraction. Stages A and B represent the electromechanical response in portions far enough from the electrodes. On the other side, stage C adds a portion of matrix in series with the homogeneous material obtained with A and B stages and introduces electric effects only relative to the electric field in the fiber as function of the electric potential applied to the electrodes. The amount of electric field achieving the fiber is mainly influenced by the matrix/fiber dielectric properties relation and by electrode fingers width and separation [15,36].

3.2. Homogenization model for the piezoelectric composite (PCHM)

A general non linear model for piezoelectric fiber reinforced composites polarized with interdigitated electrodes is presented in this paper. The model is obtained as a generalization of classical mixture theory taking into account the relations between the

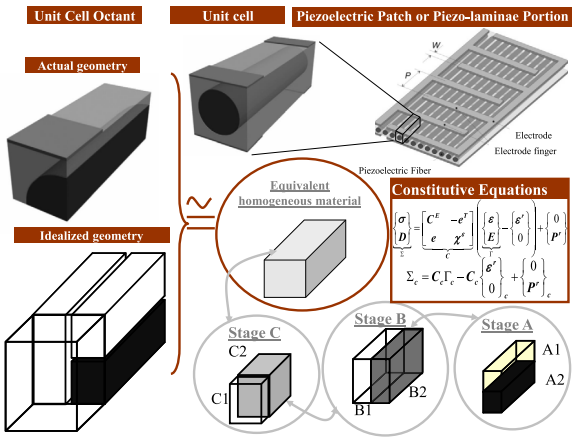

Fig. 3. Piezoelectric composite and homogenization stages.

strains, stresses, electric field, electric displacement and polarization in the components. The aforementioned relations are expressed in principal symmetry directions of the material. The homogenization model is based on Reuss and Voigt theories and on the uniform field model proposed by Bent and Hagood [15] for the linear range. Based on these approaches Luccioni [30] proposes a systematic model to make series and parallel combinations of non-linear mechanical models. In this work an extension of this last approach is presented in order to include the electric field and to take into account the non-linear electromechanical behavior of the piezoelectric/ferroelectric composites. Although the model in this paper is applied to fiber reinforced composites polarized with interdigitated electrodes, the general non-linear piezoelectric composite approach proposed is applicable to a wide variety of composite with non-linear behavior.

In order to take into account the non-linear phenomena, e.g. re-polarization, saturation and electromechanical coupling variation, all the field variables must be known for each material phase at every load increment. The deformations and electric field in the piezoelectric fibers are obtained from those of the composite by a so-called decomposition procedure. After these quantities are calculated, the constitutive equations in each constituent are integrated and then, the updated composite field variables are determined through a re-composition procedure.

The aforementioned procedure suggests the convenience of developing a well suited organized numerical tool to systematize the calculations. Having this objective in mind, based on Luccioni [30] original work and extending it to include electromechanical coupling, an alternative way of expressing the constitutive equation of each constituent is proposed in this paper. Using this approach, the composite behavior can be obtained in a relative simple manner introducing hypothesis similar to those of the classic mixture theory [26]. Regarding each field variable, strain, electric field, mechanical stress and electric displacement the material could work in series or parallel, depending on the relative disposition of each phase. The relation among the values of these variables in the components and in the composite is established based on its nature or physical properties. In this scenario it could be stated that the mechanical stresses and electric displacement on one side and strains and electric field on the other side behave in analogous way. In the directions in which the phases are disposed in series, the stress and electric displacement maintain the same value in both phases. In the directions in which the material phases are disposed in parallel, the composite stresses and electric displacement are obtained as combination of the quantities of each material phase multiplied by its volume fraction. In a similar way, in the directions in which the components are disposed in parallel, the strains and electric field maintain the same value in both phases, while in the directions in which components are disposed in series, the composite values are obtained as combination of those corresponding to each phase multiplied by its volume fraction. The aforementioned behavior of the involved physical quantities and the expressions used to calculate them are summarized in Table 1.

For the subsequent mathematical developments a symbolic matrix–vector notation is introduced. The symbolic entities encompass the physical tensor and vector components arranged in a convenient manner. Stress tensor components are arranged in vector $\boldsymbol{\sigma} = \{\sigma_{11}, \sigma_{22}, \sigma_{33}, \sigma_{12}, \sigma_{13}, \sigma_{23}\}^T$, while engineering strain components are ordered as $\boldsymbol{\varepsilon} = \{\varepsilon_{11}, \varepsilon_{22}, \varepsilon_{33}, 2\varepsilon_{12}, 2\varepsilon_{13}, 2\varepsilon_{23}\}^T$. Finally, the following arrangement results,

$$\boldsymbol{\Sigma} = \begin{Bmatrix} \boldsymbol{\sigma} \\ \mathbf{D} \end{Bmatrix}; \quad \boldsymbol{\Gamma} = \begin{Bmatrix} \boldsymbol{\varepsilon} \\ \mathbf{E} \end{Bmatrix} \tag{7}$$

The constitutive equation is stated as,

$$\begin{Bmatrix} \boldsymbol{\sigma} \\ \mathbf{D} \end{Bmatrix} = \begin{bmatrix} \mathbf{C}^E & -\mathbf{e}^T \\ \mathbf{e} & \boldsymbol{\chi}^\varepsilon \end{bmatrix} \begin{Bmatrix} \boldsymbol{\varepsilon} \\ \mathbf{E} \end{Bmatrix} - \begin{bmatrix} \mathbf{C}^E & -\mathbf{e}^T \\ \mathbf{e} & \boldsymbol{\chi}^\varepsilon \end{bmatrix} \begin{Bmatrix} \boldsymbol{\varepsilon}^r \\ \mathbf{0} \end{Bmatrix} + \begin{Bmatrix} \mathbf{0} \\ \mathbf{P}^r \end{Bmatrix} \tag{8}$$

$$\boldsymbol{\Sigma} = \mathbf{C}\boldsymbol{\Gamma} - \mathbf{C}\begin{Bmatrix} \boldsymbol{\varepsilon}^r \\ \mathbf{0} \end{Bmatrix} + \begin{Bmatrix} \mathbf{0} \\ \mathbf{P}^r \end{Bmatrix} = \mathbf{C}\hat{\boldsymbol{\Gamma}} - \begin{Bmatrix} \mathbf{0} \\ \mathbf{P}^r \end{Bmatrix} \tag{9}$$

In the preceding equation the following variable change was introduced,

$$\hat{\boldsymbol{\Gamma}} = \boldsymbol{\Gamma} - \begin{Bmatrix} \boldsymbol{\varepsilon}^r \\ \mathbf{0} \end{Bmatrix} \tag{10}$$

$\boldsymbol{\Sigma}$ and $\boldsymbol{\Gamma}$ components are rearranged as follows,

$$\boldsymbol{\Sigma}^* = \boldsymbol{\alpha}^\Sigma \boldsymbol{\Sigma} + \boldsymbol{\alpha}^\Gamma \boldsymbol{\Gamma} \tag{11}$$

$$\boldsymbol{\Gamma}^* = \boldsymbol{\alpha}^\Gamma \boldsymbol{\Sigma} + \boldsymbol{\alpha}^\Sigma \boldsymbol{\Gamma} \tag{12}$$

where $\boldsymbol{\alpha}^\Sigma$ is a diagonal tensor whose diagonal elements are 1 when the corresponding stress (strain) or electric displacement (electric field) component work in parallel (series) or 0 when the corresponding stress (strain) or electric displacement (electric field) component work in series (parallel). In a similar manner, $\boldsymbol{\alpha}^\Gamma$ is a diagonal tensor whose diagonal elements are 1 or 0 when the corresponding stress (strain) or electric displacement (electric field) component work in series (parallel) or parallel (series). The equality $\boldsymbol{\alpha}^\Sigma + \boldsymbol{\alpha}^\Gamma = \mathbf{I}$ holds.

With the operations defined in Eqs. (11) and (12), the variables that maintain the same value in both phases and the composite ($\boldsymbol{\Gamma}^*$) are separated from those that should be obtained by a combination of each phase contribution ($\boldsymbol{\Sigma}^*$). In a similar way, Eqs. (11) and (12) can be inversely written as,

$$\boldsymbol{\Sigma} = \boldsymbol{\alpha}^\Sigma \boldsymbol{\Sigma}^* + \boldsymbol{\alpha}^\Gamma \boldsymbol{\Gamma}^* \tag{13}$$

$$\boldsymbol{\Gamma} = \boldsymbol{\alpha}^\Gamma \boldsymbol{\Sigma}^* + \boldsymbol{\alpha}^\Sigma \boldsymbol{\Gamma}^* \tag{14}$$

$\boldsymbol{\Sigma}^*$ groups the stresses and electric displacement components acting in parallel and strain and electric field components acting in series. $\boldsymbol{\Gamma}^*$ encompasses strain and electric field components acting in parallel and stress and electric displacement acting in series. Combining Eq. (11) with Eqs. (9) and (10) the following relation is obtained:

$$\boldsymbol{\Sigma}^* = \boldsymbol{\alpha}^\Sigma \left[\mathbf{C}\hat{\boldsymbol{\Gamma}} + \begin{Bmatrix} \mathbf{0} \\ \mathbf{P}^r \end{Bmatrix} \right] + \boldsymbol{\alpha}^\Gamma \hat{\boldsymbol{\Gamma}} + \boldsymbol{\alpha}^\Gamma \begin{Bmatrix} \boldsymbol{\varepsilon}^r \\ \mathbf{0} \end{Bmatrix} \tag{15}$$

After a rearrangement results,

$$\boldsymbol{\Sigma}^* = \left(\boldsymbol{\alpha}^\Sigma \mathbf{C} + \boldsymbol{\alpha}^\Gamma\right) \hat{\boldsymbol{\Gamma}} + \boldsymbol{\alpha}^\Sigma \begin{Bmatrix} \mathbf{0} \\ \mathbf{P}^r \end{Bmatrix} + \boldsymbol{\alpha}^E \begin{Bmatrix} \boldsymbol{\varepsilon}^r \\ \mathbf{0} \end{Bmatrix} \tag{16}$$

In a similar manner, after combining Eq. (11) with Eqs. (8) and (9), the following expression is obtained,

$$\boldsymbol{\Gamma}^* = \left(\boldsymbol{\alpha}^\Gamma \mathbf{C} + \boldsymbol{\alpha}^\Sigma\right) \hat{\boldsymbol{\Gamma}} + \boldsymbol{\alpha}^\Gamma \begin{Bmatrix} \mathbf{0} \\ \mathbf{P}^r \end{Bmatrix} + \boldsymbol{\alpha}^\Sigma \begin{Bmatrix} \boldsymbol{\varepsilon}^r \\ \mathbf{0} \end{Bmatrix} \tag{17}$$

Clearing $\hat{\boldsymbol{\Gamma}}$ from Eq. (17), replacing it in Eq. (16) and making some algebraic operations it results,

$$\boldsymbol{\Sigma}^* = \mathbf{C}^* \boldsymbol{\Gamma}^* - \mathbf{C}^* \boldsymbol{\alpha}^\Gamma \begin{Bmatrix} \mathbf{0} \\ \mathbf{P}^r \end{Bmatrix} - \mathbf{C}^* \boldsymbol{\alpha}^\Sigma \begin{Bmatrix} \boldsymbol{\varepsilon}^r \\ \mathbf{0} \end{Bmatrix} + \boldsymbol{\alpha}^\Sigma \begin{Bmatrix} \mathbf{0} \\ \mathbf{P}^r \end{Bmatrix} + \boldsymbol{\alpha}^\Gamma \begin{Bmatrix} \boldsymbol{\varepsilon}^r \\ \mathbf{0} \end{Bmatrix} \tag{18}$$

Table 1
Variables combination mode.

Variable	Voigt (Parallel)	Reuss (Series)
$\boldsymbol{\sigma}$	$\sum k_c \boldsymbol{\sigma}_c$	Same value
$\mathbf{D}$	$\sum k_c \mathbf{D}_c$	Same value
$\boldsymbol{\varepsilon}$	Same value	$\sum k_c \boldsymbol{\varepsilon}_c$
$\mathbf{E}$	Same value	$\sum k_c \mathbf{E}_c$

where

$$\mathbf{C}^* = \left(\boldsymbol{\alpha}^{\Sigma}\mathbf{C} + \boldsymbol{\alpha}^{\Gamma}\right)\left(\boldsymbol{\alpha}^{\Gamma}\mathbf{C} + \boldsymbol{\alpha}^{\Sigma}\right)^{-1} \tag{19}$$

The preceding equations are valid both, for the composite and for a particular constituent. To make a distinction, sub-index c is introduced when referring to a constituent.

Taking into consideration that $\boldsymbol{\Sigma}^*$ has stress and electric displacement components acting in parallel and strain and electric field acting in series, $\boldsymbol{\Sigma}^*$ corresponding to the composite is obtained as a superposition of all material phases multiplied by its respective volume fraction,

$$\boldsymbol{\Sigma}^* = \sum_{c=1} k_c \boldsymbol{\Sigma}_c^* \tag{20}$$

Operating,

$$\begin{aligned}\boldsymbol{\Sigma}^* = &\left(\sum_{c=1} k_c \mathbf{C}_c^*\right)\boldsymbol{\Gamma}^* - \sum_{c=1} k_c \left[\mathbf{C}_c^*\boldsymbol{\alpha}^{\Gamma} - \boldsymbol{\alpha}^{\Sigma}\right]\left\{\begin{array}{c}\mathbf{0}\\ \mathbf{P}^r\end{array}\right\}_c \\ &- \sum_{c=1} k_c \left[\mathbf{C}_c^*\boldsymbol{\alpha}^{\Sigma} - \boldsymbol{\alpha}^{\Gamma}\right]\left\{\begin{array}{c}\boldsymbol{\varepsilon}^r\\ \mathbf{0}\end{array}\right\}_c\end{aligned} \tag{21}$$

In the last expression, $\boldsymbol{\Gamma}^*$ contains strain, stress, electric field and electric displacement components common to all composite components.

Expression (21) can be stated as,

$$\boldsymbol{\Sigma}^* = \mathbf{C}^*\boldsymbol{\Gamma}^* - \boldsymbol{\Sigma}^{*r} \tag{22}$$

where

$$\boldsymbol{\Sigma}^{*r} = \sum_{c=1} k_c \boldsymbol{\Sigma}_c^{*r} \tag{23}$$

and

$$\boldsymbol{\Sigma}_c^{*r} = \left[\mathbf{C}_c^*\boldsymbol{\alpha}^{\Gamma} - \boldsymbol{\alpha}^{\Sigma}\right]\left\{\begin{array}{c}\mathbf{0}\\ \mathbf{P}^r\end{array}\right\}_c + \left[\mathbf{C}_c^*\boldsymbol{\alpha}^{\Sigma} - \boldsymbol{\alpha}^{\Gamma}\right]\left\{\begin{array}{c}\boldsymbol{\varepsilon}^r\\ \mathbf{0}\end{array}\right\}_c \tag{24}$$

and

$$\mathbf{C}^* = \sum_{c=1} k_c \mathbf{C}_c^* \tag{25}$$

The stresses and electric displacement corresponding to the composite are grouped in $\boldsymbol{\Sigma}$ and can be calculated with the aid of Eqs. (13) and (14),

$$\boldsymbol{\Sigma} = \boldsymbol{\alpha}^{\sigma}\left[\mathbf{C}^*\boldsymbol{\Gamma}^* - \boldsymbol{\Sigma}^{*r}\right] + \boldsymbol{\alpha}^{\Gamma}\boldsymbol{\Gamma}^* = \left[\boldsymbol{\alpha}^{\Sigma}\mathbf{C}^* + \boldsymbol{\alpha}^{\Gamma}\right]\boldsymbol{\Gamma}^* - \boldsymbol{\alpha}^{\Sigma}\boldsymbol{\Sigma}^{*r} \tag{26}$$

and

$$\boldsymbol{\Gamma} = \boldsymbol{\alpha}^{\Gamma}\left[\mathbf{C}^*\boldsymbol{\Gamma}^* - \boldsymbol{\Sigma}^{*r}\right] + \boldsymbol{\alpha}^{\Sigma}\boldsymbol{\Gamma}^* = \left[\boldsymbol{\alpha}^{\Gamma}\mathbf{C}^* + \boldsymbol{\alpha}^{\Sigma}\right]\boldsymbol{\Gamma}^* - \boldsymbol{\alpha}^{\Gamma}\boldsymbol{\Sigma}^{*r} \tag{27}$$

From Eqs. (26) and (27) it results,

$$\boldsymbol{\Gamma}^* = \left(\boldsymbol{\alpha}^{\Gamma}\mathbf{C}^* + \boldsymbol{\alpha}^{\Sigma}\right)^{-1}\left(\boldsymbol{\Gamma} + \boldsymbol{\alpha}^{\Gamma}\boldsymbol{\Sigma}^{*r}\right) \tag{28}$$

Replacing Eq. (28) in (26) the following constitutive equation for the composite is obtained

$$\boldsymbol{\Sigma} = \mathbf{C}\boldsymbol{\Gamma} - \boldsymbol{\Sigma}^r \tag{29}$$

where

$$\mathbf{C} = \left(\boldsymbol{\alpha}^{\Sigma}\mathbf{C}^* + \boldsymbol{\alpha}^{\Gamma}\right)\left(\boldsymbol{\alpha}^{\Gamma}\mathbf{C}^* + \boldsymbol{\alpha}^{\Sigma}\right)^{-1} \tag{30}$$

and

$$\boldsymbol{\Sigma}^r = \left(\boldsymbol{\alpha}^{\Sigma} - \mathbf{C}\boldsymbol{\alpha}^{\Gamma}\right)\boldsymbol{\Sigma}^{*r} \tag{31}$$

To analyze the composite behavior in presence of material non-linear behavior, such as polarization switching and saturation, it is necessary to know the strains and electric field for each material phase. These variables can be determined in terms of the corresponding quantities of the composite. From the condition $\boldsymbol{\Gamma}_c^* = \boldsymbol{\Gamma}^*$ and expressions (11) and (12), the following relation can be stated for each material phase or constituent,

$$\begin{aligned}\boldsymbol{\Gamma}_c &= \boldsymbol{\alpha}^{\Gamma}\boldsymbol{\Sigma}_c^* + \boldsymbol{\alpha}^{\Sigma}\boldsymbol{\Gamma}_c^* = \boldsymbol{\alpha}^{\Gamma}\left(\mathbf{C}_c^*\boldsymbol{\Gamma}_c^* - \boldsymbol{\Sigma}_c^{*r}\right) + \boldsymbol{\alpha}^{\Sigma}\boldsymbol{\Gamma}_c^* \\ &= \left(\boldsymbol{\alpha}^{\Gamma}\mathbf{C}_c^* + \boldsymbol{\alpha}^{\Sigma}\right)\boldsymbol{\Gamma}^* - \boldsymbol{\alpha}^{\Gamma}\boldsymbol{\Sigma}_c^{*r}\end{aligned} \tag{32}$$

Taking into account Eq. (28),

$$\boldsymbol{\Gamma}_c = \boldsymbol{\phi}_c\boldsymbol{\Gamma} + \widetilde{\boldsymbol{\Gamma}}_c^r \tag{33}$$

where

$$\boldsymbol{\phi}_c = \left(\boldsymbol{\alpha}^{\Gamma}\mathbf{C}_c^* + \boldsymbol{\alpha}^{\Sigma}\right)\left(\boldsymbol{\alpha}^{\Gamma}\mathbf{C}^* + \boldsymbol{\alpha}^{\Sigma}\right)^{-1} \tag{34}$$

and

$$\widetilde{\boldsymbol{\Gamma}}_c^r = \boldsymbol{\phi}_c\boldsymbol{\alpha}^E\boldsymbol{\Sigma}^{*r} - \boldsymbol{\alpha}^{\Gamma}\boldsymbol{\Sigma}_c^{*r} \tag{35}$$

3.3. Constituent material models

For the composite being modeled, two phases are present. One corresponds to the polymeric matrix and the other one to the piezoelectric fiber. The matrix is modeled as mechanically linear elastic and electrically linear with no repolarization and hysteresis. On the other side, a phenomenological thermodynamically consistent ferroelectric model is used to describe the fiber behavior, since switching, hysteresis and repolarization processes are intended to be modeled.

Phenomenological ferroelectric switching models are addressed by Cocks and McMeeking [37], Kamlah and Tsakmakis [38], Huber and Fleck [34], Landis [39] and Semenov et al. [40], to name a few. The phenomenological constitutive model presented by Huber and Fleck [34] is used in this work. A complete description of the thermodynamical framework can be found, for instance, in [39,41]. In general terms, the phenomenological model consists of a switching surface and evolution rules for the internal variables. The switching surface defines the loading state and indicates when switching processes take place.

The switching surface is defined in the space of $\widehat{\mathbf{S}} = \mathbf{S} - \mathbf{S_o}$ and $\widehat{\mathbf{E}} = \mathbf{E} - \mathbf{E_o}$,

$$G\left(\widehat{\mathbf{S}}, \widehat{\mathbf{E}}; \mathbf{P^r}, \boldsymbol{\varepsilon}^r\right) - G_c \leqslant 0 \tag{36}$$

where $\mathbf{S}$ is the deviatoric part of stress tensor $\boldsymbol{\sigma}$ (in indicial notation $s_{ij} = \sigma_{ij} - \delta_{ij}\sigma_{kk}/3$). The quantities $\mathbf{S_o}$ and $\mathbf{E_o}$ define the switching surface centre and G_c is the critical switching value. The condition $G - G_c < 0$ implies that the material experiments no switching. During repolarization $G - G_c = 0$. Cases in which $G - G_c > 0$ are inadmissible.

As proposed by Huber and Fleck [34], the following switching surface is used in this work,

$$G^2 = \alpha^f \hat{s}_e^2 + \left|\widehat{\mathbf{E}}\right|^2 + \beta^f \widehat{\mathbf{E}} \cdot \mathbf{P}^r \cdot \widehat{\mathbf{S}} = \alpha^f \hat{s}_e^2 + \widehat{E}_i\widehat{E}_i + \beta^f \widehat{S}_{ij}\widehat{E}_i P_j^r \tag{37}$$

where

$$\hat{s}_e = \sqrt{\frac{3}{2}\widehat{\mathbf{S}} : \widehat{\mathbf{S}}} \tag{38}$$

$$\widehat{\mathbf{S}} = \mathbf{S} - \mathbf{S_o} \tag{39}$$

and

$$\widehat{\mathbf{E}} = \mathbf{E} - \mathbf{E_o} \tag{40}$$

As indicated by experimental observations, an electric field application from a non polarized initial state can indeed introduce a remanent strain state [42]. The third term of the switching function (Eq. (37)) introduces a coupling between mechanical and electrical terms and it is activated when remanent polarization takes place. The scalars α^f and β^f are constants introduced for dimensional consistency purposes, allowing model predictions calibration with experimental tests.

The switching surface centre $(\mathbf{S_o}, \mathbf{E_o})$ evolves according to the following rules:

$$\dot{\mathbf{S}}_\mathbf{o} = h_s(\boldsymbol{\varepsilon}^r)\dot{\boldsymbol{\varepsilon}}^r \tag{41}$$

and

$$\dot{\mathbf{E}}_\mathbf{o} = h_e(\mathbf{P}^r)\dot{\mathbf{P}}^r \tag{42}$$

where $h_s(\boldsymbol{\varepsilon}^r)$ and $h_e(\mathbf{P}^r)$ are scalar functions of remanent strain and polarization, respectively. Expressions for $h_s(\boldsymbol{\varepsilon}^r)$ and $h_e(\mathbf{P}^r)$ are chosen so that high values of hardening are obtained when approaching saturation,

$$h_s(\boldsymbol{\varepsilon}^r) = h_{0s}\left(1 - \frac{\frac{I_2}{4}\left(3 - \left(\frac{I_3}{I_2}\right)^3\right)}{\varepsilon_{sat}}\right)^{-n_s} \tag{43}$$

$$h_e(\mathbf{P}^r) = h_{0e}\left(1 - \frac{|\mathbf{P}^r|}{P_{sat}}\right)^{-n_e} \tag{44}$$

where I_2 e I_3 are the second and third invariants of remanent deformation tensor $\boldsymbol{\varepsilon}^r$; h_{0e} and h_{0s} are initial hardening rates while n_s and n_e are exponents regulating the hardening rate, lock-up and response shape. P_{sat} and ε_{sat} are saturation remanent polarization and deformation, respectively.

An associative flow rule is used for $\boldsymbol{\varepsilon}^r$ and $\mathbf{P}^r$, according to that

$$\dot{\mathbf{P}}^r = \dot{\lambda}\frac{\partial G}{\partial \widehat{\mathbf{E}}} \tag{45}$$

and

$$\dot{\boldsymbol{\varepsilon}}^r = \dot{\lambda}\frac{\partial G}{\partial \widehat{\mathbf{S}}} \tag{46}$$

where $\dot{\lambda} > 0$ implies switching process and $\dot{\lambda} = 0$ means linear response.

To integrate the constitutive ferroelectric switching equations corresponding to the fibers, a class of return-mapping algorithm, called cutting-plane scheme [43] is implemented along with the proposed composite model. The constitutive equation integration is derived in Section 4.3.

3.4. Composite calculation scheme

In the preceding development and for the successive calculations corresponding to the composite, a decomposition process followed by a composition one is clearly distinguished. Based on nodal mechanical displacements and electric potentials, deformations and electric field are calculated. These quantities are decomposed up to determine the corresponding values soliciting the piezoelectric fibers and with these values the constitutive equations are integrated. After material properties update, internal variables and state of the material, stress and electric displacement are updated. This is the starting point to the re-composition process for the updated composite state calculation. The process is schematically summarized in Fig. 4 using the same colors of Fig. 3.

Due to the non linear nature of the problem (the term $\widetilde{\boldsymbol{\Gamma}}_c^r$ of Eq. (33) is not known in advance) the decomposition process should be done in an iterative way [30] or with an explicit advancing scheme. Due to the complexity and high non linearity of the problem involved, the last approach with control of critical time step is used in this work. Decomposition/Composition (D/C) processes are performed in 3 stages. In each D/C stage two components are involved. D/C process is detailed in the next section.

4. Numerical implementation

The proposed PCHM has been implemented and included in ABAQUS. Since, the main contribution of the present article is related to the constitutive model itself it could be implemented in ABAQUS via the UMAT user subroutine. Nevertheless, at the moment UMAT does not support electric variables in its interface. Thus, the material model implementation has been made by embedding it inside the USER ELEMENT subroutine (UEL) of the piezoelectric shell finite element originally proposed by Guennam and Luccioni [44]. The integration of the material model with the aforementioned shell element provide a tool for modeling piezoelectric laminates in non linear material range.

PCHM results are compared with a detailed unit cell model (UCDM). The UCDM is an explicit FE discretization of the piezo-composite RVE. In order to construct the FE/UCDM, a piezoelectric solid brick finite element has also been implemented as a

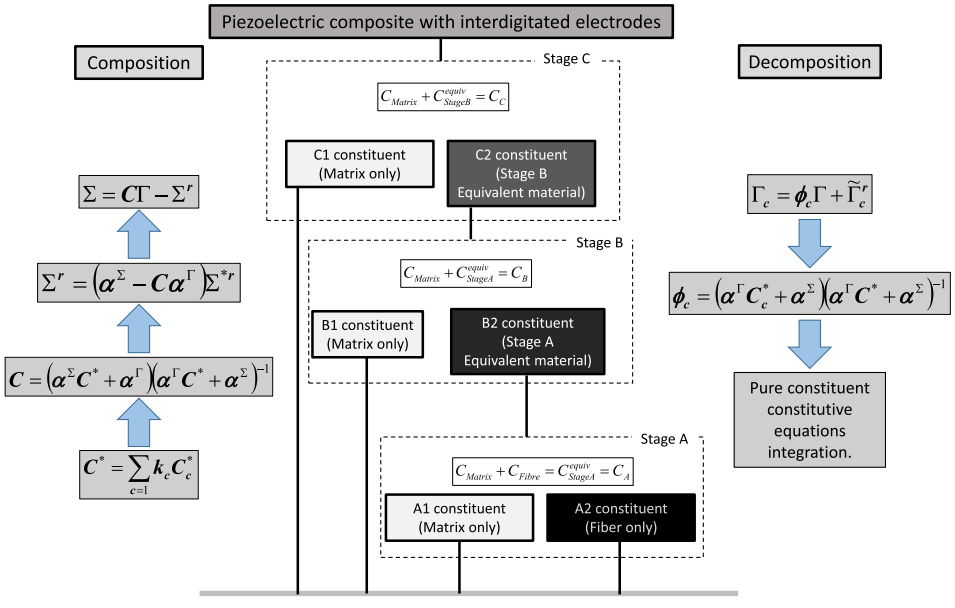

Fig. 4. Decomposition and composition scheme.

UEL subroutine including the same constitutive model for pure piezoelectric/ferroelectric materials used in the PCHM.

The whole code of the numerical tools developed and used in this work is organized in a modular way in order to facilitate the maintenance, debugging and code reuse. The principal modules are:

- Piezoelectric shell module
- Piezoelectric solid 3D brick module
- Piezo-composite homogenization model (PCHM) module
- Constitutive module for pure piezoelectric/ferroelectric materials using a cutting plane return mapping algorithm.

A scheme of the tools developed and implemented along this work is depicted in Fig. 5.

Besides the homogenization model itself, two main ingredients can be identified in this work, namely the integration of the pure material constitutive equation and the FE implementation.

4.1. Non linear FE generalities

Non linear FE formulation is widely explained in the specialized bibliography. Therefore, only the features necessary to explain the framework of the numerical implementation of the proposed model are presented. According to physics laws, for a body to be in equilibrium, internal and external *forces* must be balanced. This is expressed as,

$$\mathbf{F}^{int} - \mathbf{F}^{ext} = 0 \tag{47}$$

Physical nature of *forces* depends on the problem being considered. For the case of piezoelectric analysis, the term *force* includes mechanical forces and moments as well as electric charges. Moreover, as stated in Section 3.2, mechanical stresses and electric displacement are grouped in vector $\mathbf{\Sigma} = \{\boldsymbol{\sigma}, \mathbf{D}\}^T$ and strains and electric field are grouped in vector $\mathbf{\Gamma} = \{\boldsymbol{\varepsilon}, \mathbf{E}\}^T$.

In finite elements procedures, nodal *displacements* are defined. For the problem being considered, nodal *displacements* are grouped in vector $\mathbf{d} = \{\mathbf{u}, \phi\}^T$, where $\boldsymbol{u}$ includes mechanical displacements and rotations, while ϕ corresponds to electric potentials. The formulation used and the type of element considered define a matrix operator relating $\mathbf{d}$ with $\mathbf{\Gamma}$,

$$\mathbf{\Gamma} = \mathbf{B}\mathbf{d} \tag{48}$$

Thus, internal force vector is calculated as

$$\mathbf{F}^{int} = \int_{V_e} \mathbf{B}^T \mathbf{\Sigma} dV \tag{49}$$

In a non-linear quasi-static incremental analysis, equality (47) must be verified at every load increment n. Provided that equilibrium at increment n is verified, the equilibrium state at $n+1$ must be found. If there are unbalanced forces at $n+1$, a residual $\mathbf{R}^{(k)}_{n+1} = \mathbf{F}^{int\,(k)}_{n+1} - \mathbf{F}^{ext}_{n+1}$ is obtained. Using a Newton–Raphson approach, nodal displacement increments $\Delta\mathbf{d}^{(k+1)}_{n+1}$ are estimated as follows:

$$\Delta\mathbf{d}^{(k+1)}_{n+1} = -\left[\frac{\partial \mathbf{R}^{(k)}}{\partial \mathbf{d}_{n+1}}\right]^{-1} \left\{\mathbf{F}^{int\,(k)}_{n+1} - \mathbf{F}^{ext}_{n+1}\right\} \tag{50}$$

Updating nodal displacements as $\mathbf{d}^{(k+1)}_{n+1} = \mathbf{d}^{(k)}_{n+1} + \Delta\mathbf{d}^{(k+1)}_{n+1}$, $\mathbf{F}^{int}$ can be recalculated and the iteration process continues until $\mathbf{R}^{(k+1)}_{n+1} \leqslant TOL$.

As described in ABAQUS/User Subroutines manual, UEL subroutine must compute the contributions of the element to the global system of equations [35]. For the analysis being described, UEL must return $\frac{\partial \mathbf{R}^{(k)}}{\partial \mathbf{d}_{n+1}}$ or an approximation to it in AMATRX array, $\int_{V_e} \mathbf{B}^T \mathbf{\Sigma} dV$ in RHS and update all the internal variables involved in SVARS. The calculation of the tangent matrix

$$\frac{\partial \mathbf{R}^{(k)}}{\partial \mathbf{d}_{n+1}} = \sum_{e=1}^{ne} \int_{V_e} \mathbf{B}^T \frac{\partial \mathbf{\Sigma}^{(k)}_{n+1}}{\partial \mathbf{\Gamma}^{(k)}_{n+1}} \mathbf{B} dV \tag{51}$$

is needed if quadratic convergence rate is pursued. This calculation could be cumbersome or even impossible, depending on the complexities involved [45]. Alternatively, quasi-Newton methods could be used [45]. In this work, $\frac{\partial \mathbf{\Sigma}^{(k)}_{n+1}}{\partial \mathbf{\Gamma}^{(k)}_{n+1}}$ is approximated with the secant constitutive tensors updated according to remanent quantities evolution. As discussed in [46,45], a very attractive alternative is a numerical evaluation of tangent modulus. The inclusion of this approach in the proposed formulation is being considered.

Special attention is paid in the load increment marching in order to reduce errors and minimize convergence issues. A load increment control and an iterative processes at structural level is performed by ABAQUS. This iterative process is called outer iteration and is denoted herein with counter k. On the other side, inside UEL an inner iteration is performed at each quadrature point when integrating the constitutive equations. The inner iteration counter is denoted with i. ABAQUS/UEL PNEWDT parameter is used to enforce a decrease in load incrementation if PCHM/CPRM algorithms detect important change in internal variables values or they achieve values outside valid limits. Moreover, if inner iteration convergence is not achieved a decrease in load increment is imposed too.

For each load increment n and outer iteration k, nodal mechanical displacements and electric potentials ϕ are calculated by ABAQUS. Inside UEL, strains and electric field $\mathbf{\Gamma} = \{\boldsymbol{\varepsilon}, \mathbf{E}\}^T$ are calculated for each quadrature point. If the material used is a piezoelectric composite a sequence of decomposition followed by the integration of the constitutive equation (CE) and finally a re-composition is triggered. If, on the other side, the material is monolithic ferroelectric, the CE is integrated directly.

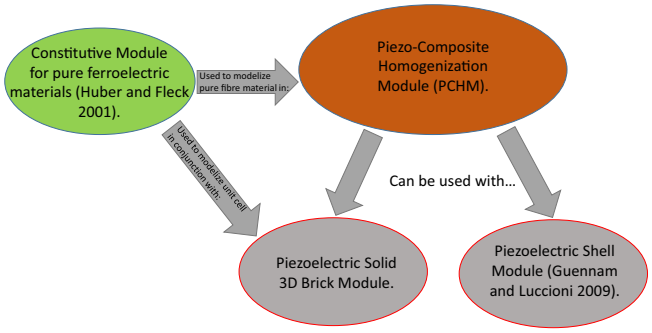

Fig. 5. Numerical tools developed/implemented in this work.

4.2. Piezo-composite homogenization model calculation sequence

As stated in Section 3.1, the composite being modeled in this work is considered as built in three stages (A, B, and C) algorithmically denoted as ($s = 1, 2, 3$). Each stage has two constituents (c_1 and c_2). Only stage A ($s = 1$) has two pure constituents, i.e. pure matrix and pure piezoelectric fiber. For stages B and C, c_1 corresponds to matrix pure material and c_2 is the sub-composite of the precedent stage.

When the PCPIE material is used in a FE model, $\mathbf{\Gamma} = \{\boldsymbol{\varepsilon}, \mathbf{E}\}^T$ obtained from Eq. (48) corresponds to the homogenized material and the decomposition process described in Section 3.2 is used to determine $\mathbf{\Gamma}^{s=1}_{c_1}$ and $\mathbf{\Gamma}^{s=1}_{c_2}$ for each pure constituent of stage $s = 1 \equiv A$. After decomposition process, the constitutive model of each pure material is used to calculate stresses σ and electric

displacements as well as remanent quantities $\mathbf{\Gamma}_{r_{c_2}}^{s=1}$ and other internal variables corresponding to component 2. Finally, a recomposition process is performed to obtain the homogenized composite properties and, $\mathbf{\Sigma} = \{\boldsymbol{\sigma}, \mathbf{D}\}^T$. The Decomposition/Composition (D/C) process is depicted in Algorithm 1. Herein it is assumed that an initial composition has been made at loading increment $n = 0$ in order to obtain a starting piezo-composite material. Algorithm 1 corresponds to a intermediate loading increment n and outer iteration k, not included to simplify the notation.

Algorithm 1: Decomposition/Composition (D/C) process.

Input: $\mathbf{\Gamma} = \{\boldsymbol{\varepsilon}, \mathbf{E}\}^T$, internal variables ($\boldsymbol{\varepsilon}^r$, $\mathbf{P}^r$, Switching surface center ($\mathbf{E}_o$ and $\mathbf{S}_o$))
Decomposition:
for $s \leftarrow n_{stages}$ ***to*** *1* **do**
  Calculate:
  $\mathbf{C}_{c_1}^{*\,s}$ and $\mathbf{C}_{c_2}^{*\,s}$ (Eq. (19))
  $\mathbf{C}^{*s}$ (Eq. (25))
  $\boldsymbol{\phi}_{c_1}^{s}$ and $\boldsymbol{\phi}_{c_2}^{s}$ (Eq. (34))
  $\mathbf{\Sigma}_{c_1}^{*rs}$ and $\mathbf{\Sigma}_{c_1}^{*rs}$ (Eq. (24))
  $\mathbf{\Sigma}^{*rs}$ (Eq. (23))
  $\tilde{\mathbf{\Gamma}}_{\mathbf{c_1}}^{r\;s}$ and $\tilde{\mathbf{\Gamma}}_{\mathbf{c_2}}^{r\;s}$ (Eq. (35))
  $\mathbf{\Gamma}_{c_1}{}^{s}$ and $\mathbf{\Gamma}_{c_2}{}^{s}$ (Eq. (33))
  if $s > 1$ **then**
    $\mathbf{\Gamma}^{s-1} \leftarrow \mathbf{\Gamma}_{c_2}{}^{s}$
Field variables ($\mathbf{\Gamma}_{c_1}^{s=1}$ and $\mathbf{\Gamma}_{c_2}^{s=1}$) of each constituent are known.
Integrate CE of each constituent using CPRM (See 4.3)
Internal state ($\boldsymbol{\varepsilon}^r$, $\mathbf{P}^r$, $\mathbf{E}_o$ and $\mathbf{S}_o$) is updated.
Composition:
$\mathbf{\Gamma}_{r_{c_2}}^{s=1} \leftarrow \boldsymbol{\varepsilon}^r, \mathbf{P}^r$, $\mathbf{\Gamma}_{r_{c_1}}^{s=1} \leftarrow 0$
$\mathbf{C}_{c_2}^{s=1} \leftarrow (\mathbf{C}^E, \mathbf{e}^T, \boldsymbol{\chi}^{\varepsilon})_{Fibre}$, $\mathbf{C}_{c_1}^{s=1} \leftarrow (\mathbf{C}^E, 0, \boldsymbol{\chi}^{\varepsilon})_{Matrix}$
for $s \leftarrow 1$ ***to*** n_{stages} **do**
  Calculate:
  $\mathbf{C}_{c_1}^{*\,s}$ and $\mathbf{C}_{c_2}^{*\,s}$ (Eq. (19))
  $\mathbf{C}^{*s}$ (Eq. (25))
  $\mathbf{C}^{s}$ (Eq. (30))
  $\mathbf{\Sigma}_{c_1}^{*rs}$ and $\mathbf{\Sigma}_{c_1}^{*rs}$ (Eq. (24))
  $\mathbf{\Sigma}^{*rs}$ (Eq. (23))
  $\mathbf{\Sigma}^{s}$ (Eq. (29))
$\boldsymbol{\sigma}, \mathbf{D} \leftarrow \mathbf{\Sigma}^{s=n_{nstages}}$
Return: $\mathbf{\Sigma}_{Composite}$, Updated $\mathbf{C} = (\mathbf{C}^E, \mathbf{e}^T, \boldsymbol{\chi}^{\varepsilon})_{Composite}$ and $\mathbf{\Gamma}^r$

4.3. Cutting plane return mapping algorithm

As stated in Section 3, in this work the model proposed by Huber and Fleck [34] is used to describe the behavior of piezoelectric fibers. Additionally, a procedure based on a cutting-plane return mapping (CPRM) method is proposed for integration of the constituent constitutive equations.

For the load increment $n+1$, the switching condition is checked at each quadrature point. If $G_{n+1} \leqslant G_c$, the behavior is linear, on the other side if $G_{n+1} > G_c$ the material experiences a switching process and the condition $G_{n+1}^{(i+1)} = G_c$ has to be restored using an iterative process. Iteration counter i is used for this process.

The switching condition is expressed as

$$G_{n+1}^{(i+1)} - G_c = 0 \tag{52}$$

Eq. (52) can be linearized as follows,

$$G_{n+1}^{(i+1)} = G_{n+1}^{(i)} + \left(\frac{\partial G}{\partial \widehat{\mathbf{S}}}\right)_{n+1}^{(i)} : \underbrace{\left(\widehat{\mathbf{S}}_{n+1}^{(i+1)} - \widehat{\mathbf{S}}_{n+1}^{(i)}\right)}_{\delta \widehat{\mathbf{S}}_{n+1}^{(i+1)}} + \left(\frac{\partial G}{\partial \widehat{\mathbf{E}}}\right)_{n+1}^{(i)} \cdot \underbrace{\left(\widehat{\mathbf{E}}_{n+1}^{(i+1)} - \widehat{\mathbf{E}}_{n+1}^{(i)}\right)}_{\delta \widehat{\mathbf{E}}_{n+1}^{(i+1)}}$$
$$+ \left(\frac{\partial G}{\partial \mathbf{P}^r}\right)_{n+1}^{(i)} \cdot \underbrace{\left(\mathbf{P}^r{}_{n+1}{}^{(i+1)} - \mathbf{P}^r{}_{n+1}{}^{(i)}\right)}_{\delta \mathbf{P}^r{}_{n+1}{}^{(i+1)}} + \left(\frac{\partial G}{\partial \boldsymbol{\varepsilon}^r}\right)_{n+1}^{(i)} : \underbrace{\left(\boldsymbol{\varepsilon}^r{}_{n+1}{}^{(i+1)} - \boldsymbol{\varepsilon}^r{}_{n+1}{}^{(i)}\right)}_{\delta \boldsymbol{\varepsilon}^r{}_{n+1}{}^{(i+1)}} \tag{53}$$

Remanent polarization and strain are updated as follows:

$$(\boldsymbol{\varepsilon}^r)_{n+1}^{(i+1)} = (\boldsymbol{\varepsilon}^r)_{n+1}^{(i)} + \underbrace{\Delta\lambda^{(i+1)} \left(\frac{\partial G}{\partial \widehat{\mathbf{S}}}\right)_{n+1}^{(i)}}_{\delta \boldsymbol{\varepsilon}^r} \tag{54}$$

and

$$(\mathbf{P}^r)_{n+1}^{(i+1)} = (\mathbf{P}^r)_{n+1}^{(i)} + \underbrace{\Delta\lambda^{(i+1)} \left(\frac{\partial G}{\partial \widehat{\mathbf{E}}}\right)_{n+1}^{(i)}}_{\delta \mathbf{P}^r} \tag{55}$$

where $\Delta\lambda = \dot{\lambda}\Delta t$.

Deviatoric stress and electric field corresponding to the center of the switching surfaces are updated as follows:

$$\mathbf{S}_{o_{n+1}}^{(i+1)} = \mathbf{S}_{o_{n+1}}^{(i)} + \underbrace{\Delta\lambda_{n+1}^{(i+1)} h_s (\boldsymbol{\varepsilon}^r)_{n+1}^{(i)} \left(\frac{\partial G}{\partial \widehat{\mathbf{S}}}\right)_{n+1}^{(i)}}_{\delta \mathbf{S}_o} \tag{56}$$

$$\mathbf{E}_{o_{n+1}}^{(i+1)} = \mathbf{E}_{o_{n+1}}^{(i)} + \underbrace{\Delta\lambda^{(i+1)} h_e (\mathbf{P}^r)_{n+1}^{(i)} \left(\frac{\partial G}{\partial \widehat{\mathbf{E}}}\right)_{n+1}^{(i)}}_{\delta \mathbf{E}_o} \tag{57}$$

Deviatoric relative stress tensor increment $\delta\widehat{\mathbf{S}}$ is calculated according to:

$$\delta \widehat{\mathbf{S}}_{n+1}^{(i+1)} = \delta \mathbf{S}_{n+1}^{(i+1)} - \delta \mathbf{S}_{o_{n+1}}^{(i+1)} \tag{58}$$

Taking into account Eqs. (1) and (56), the increment of the relative deviatoric stress is calculated as

$$\delta \widehat{\mathbf{S}}_{n+1}^{(i+1)} = \Delta\lambda^{(i+1)} \left[dev \left\{ -\mathbf{C} : \left(\frac{\partial G}{\partial \widehat{\mathbf{S}}}\right) - \left(\frac{\partial \mathbf{e}^T}{\partial \mathbf{P}^r}\right) \cdot \left(\frac{\partial G}{\partial \widehat{\mathbf{E}}}\right) \right\} - h_s \left(\frac{\partial G}{\partial \widehat{\mathbf{S}}}\right) \right]_{n+1}^{(i)} \tag{59}$$

Accordingly, relative electric field increment $\delta\widehat{\mathbf{E}}$ is calculated as,

$$\delta \widehat{\mathbf{E}}_{n+1}^{(i+1)} = -\delta \mathbf{E}_{\mathbf{o}_{n+1}}^{(i)} = -\Delta\lambda_{n+1}^{(i)} h_e (\mathbf{P}^r)_{n+1}^{(i)} \frac{\partial G^{(i)}}{\partial \widehat{\mathbf{E}}_{n+1}} \tag{60}$$

The ferroelectric multiplier $\Delta\lambda$ is calculated by replacing Eqs. (53)–(60) into Eq. (52), to obtain the following:

$$\Delta\lambda_{n+1}^{(i+1)} = \frac{G_{n+1}^{(i)} - G_c}{\left(\frac{\partial G}{\partial \widehat{\mathbf{S}}} : \left[dev \left\{ \mathbf{C} : \frac{\partial G}{\partial \widehat{\mathbf{S}}} + \frac{\partial \mathbf{e}^T}{\partial \mathbf{P}^r} \cdot \frac{\partial G}{\partial \widehat{\mathbf{E}}} \right\} + h_s \frac{\partial G}{\partial \widehat{\mathbf{S}}} \right] + h_e \frac{\partial G}{\partial \widehat{\mathbf{E}}} \cdot \frac{\partial G}{\partial \widehat{\mathbf{E}}} - \frac{\partial G}{\partial \mathbf{P}_r} \cdot \frac{\partial G}{\partial \widehat{\mathbf{E}}} \right)_{n+1}^{(i)}} \tag{61}$$

Once $\Delta\lambda_{n+1}^{(i+1)}$ is calculated, remanent variables $\boldsymbol{\varepsilon}^r$ and $\mathbf{P}^r$ are updated using Eqs. (54) and (55).

Relative stress deviatoric tensor $\widehat{\mathbf{S}}$ and relative electric field vector $\widehat{\mathbf{E}}$ are computed with Eqs. (59) and (60).

After remanent polarization is updated, the corresponding piezoelectric tensor can be determined using Eq. (3) and the updated stress and electric displacement is determined.

The process is continued until the following convergence conditions are satisfied:

$$\begin{aligned} \frac{\left| G^{(k+1)} - G_c \right|}{G_c} &\leqslant Tol_G \\ \frac{\left| \boldsymbol{\varepsilon}^{r(k+1)} - \boldsymbol{\varepsilon}^{r(k)} \right|}{\varepsilon^{sat}} &\leqslant Tol_{\varepsilon^r} \\ \frac{\left| \mathbf{P}^{r(k+1)} - \mathbf{P}^{r(k)} \right|}{P^{sat}} &\leqslant Tol_{P^r} \end{aligned} \tag{62}$$

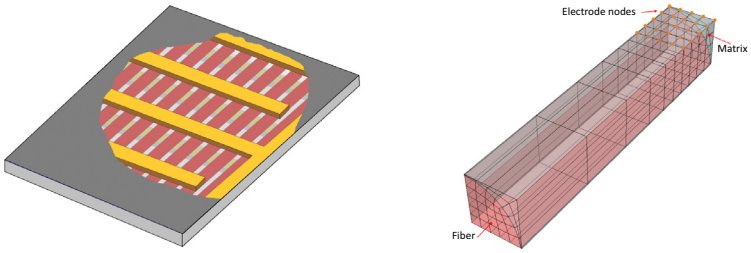

(a) Schematic piezoelectric laminae.

(b) Unit cell detailed model (UCDM) with solid elements.

Fig. 6. Piezo-composite.

5. Model validation and practical applications

Before going further into application examples the proposed homogenization approach is validated. After that, some application examples are presented.

5.1. Model validation

In order to validate the proposed homogenization model, the electromechanical response of a piezoelectric simple laminae is predicted with two approaches, on one side, using the proposed PCHM and, on the other side, with a micro-electromechanical detailed model (UCDM) consisting of an explicit finite element discretization of a representative volume element of the composite (Fig. 6). The electromechanical responses predicted by both approaches are then compared.

The PCHM as well as the UCDM use the same constitutive models for each phase, i.e. Huber and Fleck [34] phenomenological model for the fiber and linear electroelastic model for the matrix.

It is well known that fiber volume fraction (CFVF), dielectric permittivity ratio (DPR) and elastic modulus ratio (EMR) between matrix and fiber drastically affect piezoelectric composites behavior and performance [15,36]. To make sure that the proposed model is sensitive to those parameters, different values of CFVF, DPR and EMR are considered and results of both, homogenization and detailed models are compared.

Fiber material properties are summarized in Table 2.

Since the effect of elastic modulus ratio (EMR) and dielectric modulus ratio (DPR) between fiber and matrix are analyzed, the properties of the fiber are left fixed while matrix shear modulus G and κ^{σ} are changed by multiplying them by EMR and DPR, respectively.

Table 3 summarizes parameters used for fiber phenomenological model.

Fig. 7 presents the fiber portion of the unit cell analyzed with the UCDM model and the electric field arising inside it. As it can be seen, a highly 3D electric field pattern is developed under the electrode zone, whereas the electric field is almost fully fiber-wise aligned outside electrodes zone.

Table 2
Material properties for piezoelectric fiber.

Material property	Value
Poisson ratio ν	0.31
Shear modulus G (GPa)	20.8
κ^{σ} (10^{-7} F/m)	2.0
d_{33} (10^{-12} mV^{-1})	2206
d_{31} (10^{-12} mV^{-1})	−1103
d_{15} (10^{-12} mV^{-1})	2760

Table 3
Phenomenological model parameters for the fibers.

Parameter	Value
α (m^4 C^{-2})	0.0011
β (m^4 C^{-2})	0.2
h_{0e} (10^5 F^{-1} m)	714
h_{0e} (GPa)	620
n_e	1.4
n_e	1.4
G_c (MV/m)	0.82
ε_{sat} (%)	0.465
P_{sat} (C/m^2)	0.24

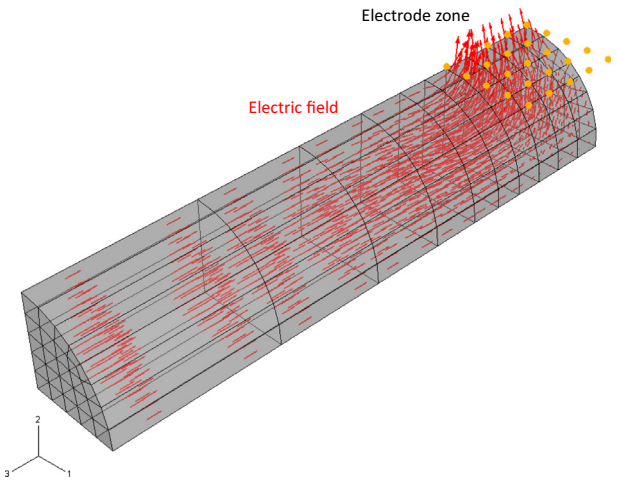

Fig. 7. Electric field inside a unit cell. 75% fiber composite. Dielectric ratio 5.0.

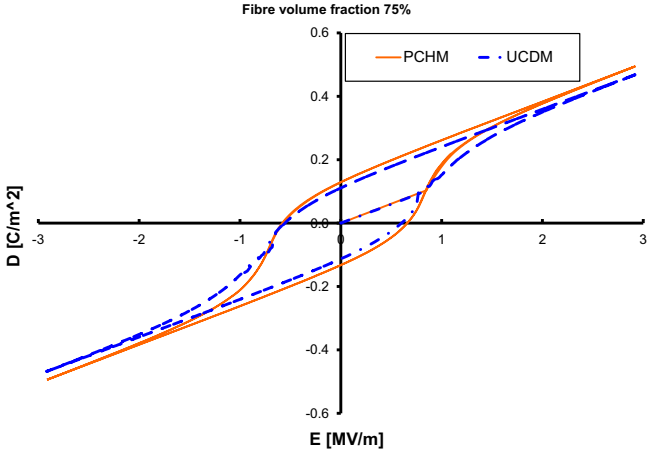

Fig. 8. Electric displacement. Composite vs detailed model results. 75% fiber composite. Dielectric ratio 5.0.

Figs. 8 and 9 show the dielectric and electromechanical response of both, PCHM and UCDM.

Figs. 8 and 9 reveal that the proposed model is able to predict the electromechanical response in good agreement with the detailed model. Differences in results are consistent with the fact that high electric field in zones near electrodes could introduce "premature switching" that can be captured by UCDM but not by PCHM which predicts average response.

To study the effect of fiber volume fraction (CFVF) on the composite electromechanical behavior, a $CFVF = 40\%$ is considered next. The results are plotted in Figs. 10 and 11.

Comparison of Figs. 10 and 11 with Figs. 8 and 9 reflect the "degradation" of the composite electromechanical response as CFVF decrease and, at the same time, a good correlation between PCHM and UCDM results.

The effect of the dielectric permittivity ratio (DPR) on piezo-composite electromechanical coupling is investigated. Results corresponding to DPR = 5, 20 and 100 are presented for both, homogenization and detailed micro-electromechanical 3D models. The responses predicted by both approaches for the three values of DPR considered are presented in Figs. 12 and 13 for comparisons.

Figs. 13 and 12 suggest that the general behavior is captured by the proposed piezo-composite model. The greatest difference in strains values predicted by both models, correspond to voltages

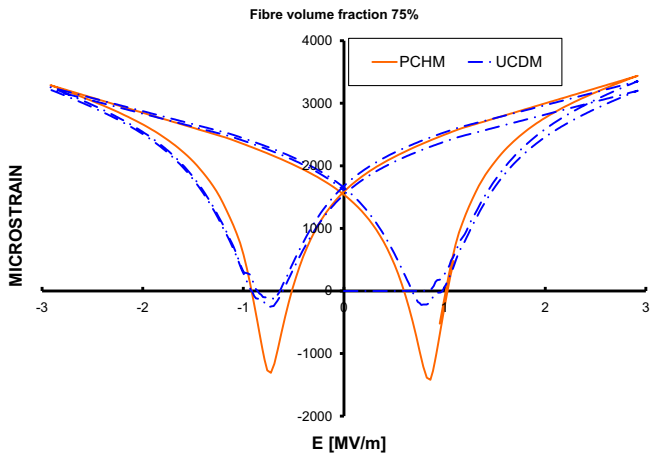

Fig. 9. Strain butterfly cycle. Composite vs detailed model results. 75% fiber composite. Dielectric ratio 5.0.

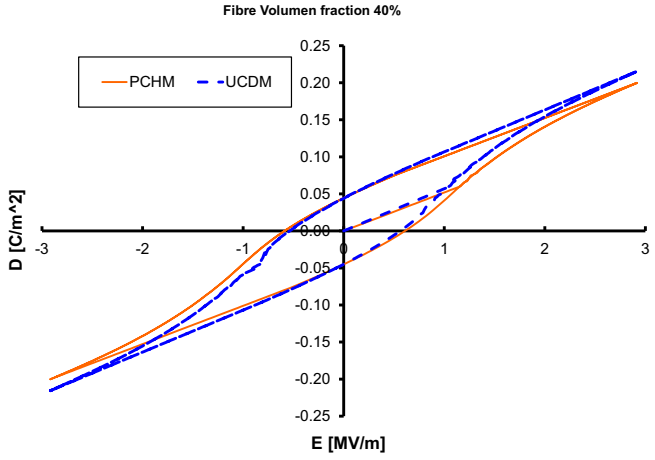

Fig. 10. Electric displacement. Composite vs detailed model results. 40% fiber composite. Dielectric ratio 5.0.

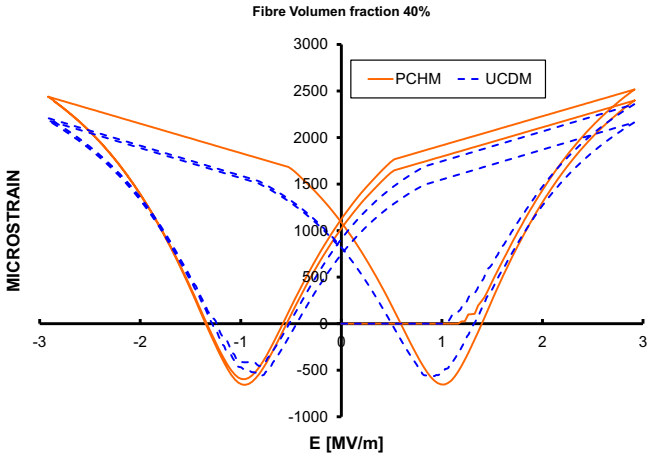

Fig. 11. Strain butterfly cycle. Composite vs detailed model results. 40% fiber composite. Dielectric ratio 5.0.

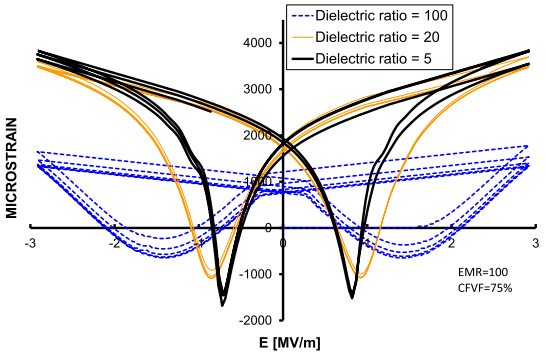

Fig. 12. Strain butterfly cycle for DPR = 5, 20 and 100. EMR = 100. 75% fiber composite. Proposed homogenization model results.

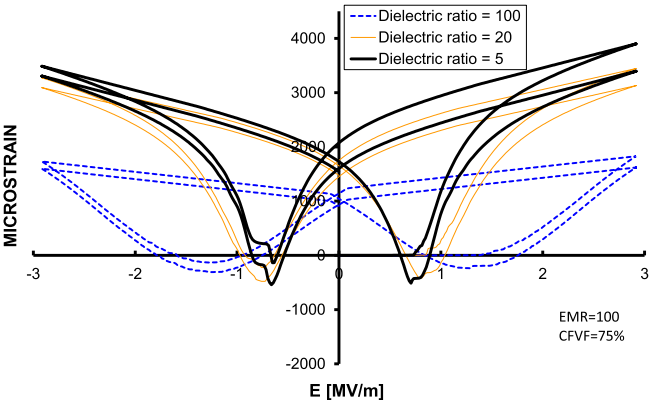

Fig. 13. Strain butterfly cycle for DPR = 5, 20 and 100. EMR = 100. 75% fiber composite. Microelectromechanical model results.

close to "yield voltage". This fact is related to the non-uniform distribution of the electric field pattern in the electrodes zone as it can be observed in Fig. 7. Besides, Fig. 13 shows some gradual switching processes predicted by the micromechanic model while Fig. 12 indicates that the homogenization model predicts the phenomena in an averaged way.

5.2. Polarization and working life cycle of a piezoelectric patch

A life cycle of a piezoelectric composite patch polarized with interdigitated electrodes is numerically studied in this application

example. The life cycle consists of an initial polling, a working cycle and finally an eventual and non desired depolarization situation caused by voltages beyond *safe* operative limits.

Fig. 14 shows that beyond de reversal electric field limit an 85% coupling loss is predicted for this composite. This is an important technical issue in piezoelectric actuator applications.

The proposed model is used to analyze the stress induced depolarization process in the piezo-composite. The response is presented in Fig. 15, where electric displacement D and remanent polarization P_r corresponding to both, UCDM and PCHM are compared.

The results are encouraging since, as shown in Fig. 15, good agreement between both approaches is observed. As predicted by monolithic material models, the composite model reflects the stress induced depolarization. The fact that a mechanical stress cannot destroy the polarization is also captured by the model.

The response of the composite after the stress depolarization is depicted in Fig. 16.

As shown in Fig. 16, the initial polling phase is identical to the former one for life cycle example. After the polling and working cycle a, compressive stress applied under zero voltage condition (path EB), causes a permanent deformation. If an electric field is applied after this point, a new butterfly response is obtained, but the predicted initial coupling is lower than that corresponding to the initial working cycle. Fig. 16 also shows that the final coupling after re-polling is almost equal to the initial coupling cycle along path EA. However, it is observed that a permanent strain remains in the device.

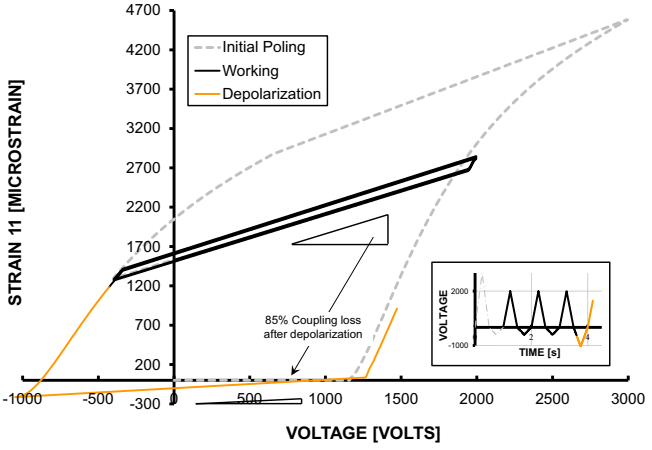

Fig. 14. Composite response under an initial polarization followed by a working cycle. After that, enough negative electric field causes depolarization.

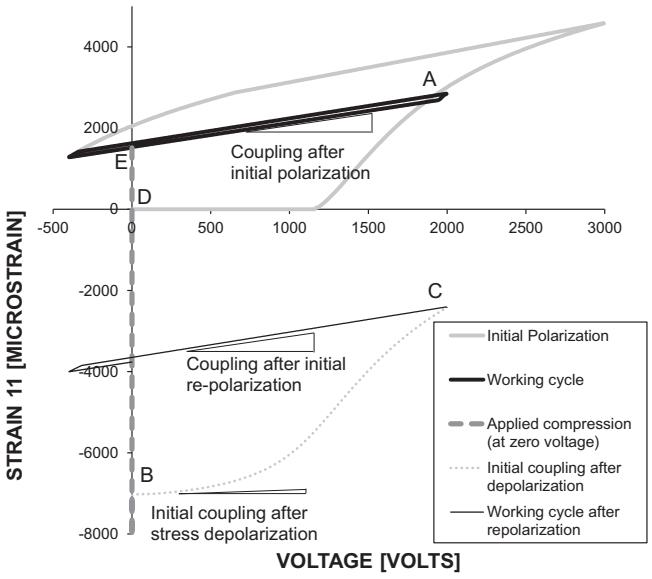

Fig. 16. Composite response against an initial polarization followed by a working cycle (A). After that, a compressive stress depolarization takes place and subsequent re-polarization (C) and working cycle after coupling recovers (B).

Finally, convergence of the numerical models is analyzed in this application example. For this purpose, the piezoelectric patch is polarized first and then, a compressive stress of 70 Mpa is applied using amplitudes shown in Fig. 17.

The number of both, outer (global equilibrium level) as well as inner (CE integration) iterations required for the convergence of the pure constituent model corresponding to PCHM and UCDM are presented in Figs. 18 and 19, respectively. As a reference, in the second axis the remanent polarization evolution is plotted. For the UCDM, the results correspond to a Gauss point of element laying on longitudinal z axis of the unit cell and opposite to electrode zone.

Figs. 18 and 19 show the correlation between switching activity and inner iterations in the cutting plane algorithm. A total of 2000 load increment was used.

As it can be observed in Fig. 18, outer iterations start sooner than their inner counterpart. This is due to the non uniform distribution of electric field along the detailed model. According to that, the switching process starts near electrodes zone while fiber portion near "z" symmetry plane is still in an unpoled condition. As

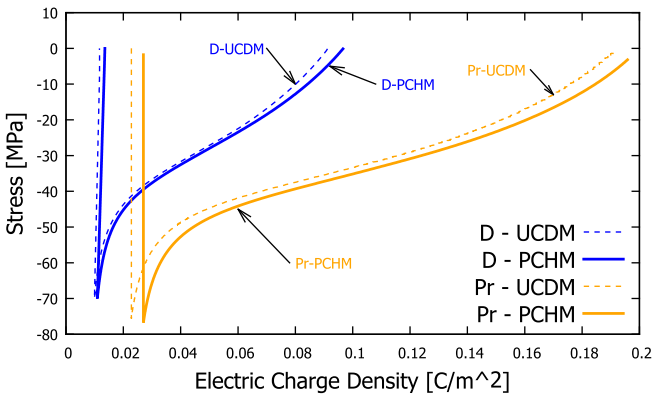

Fig. 15. Stress depolarization response.

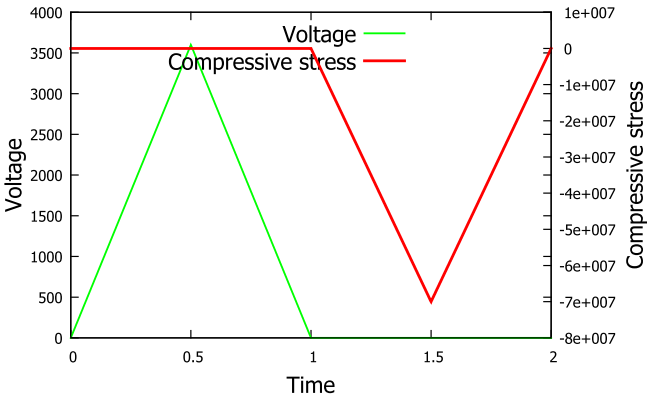

Fig. 17. Voltage and stress amplitudes.

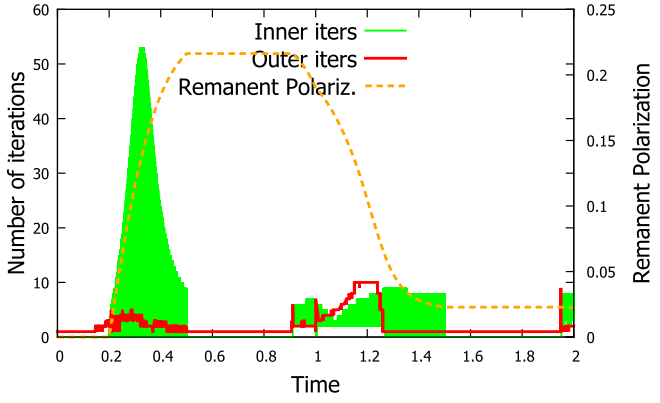

Fig. 18. UCDM convergence behavior – inner iterations.

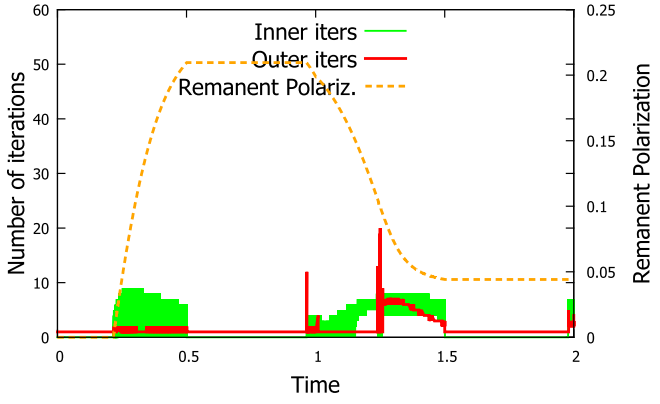

Fig. 19. PCHM convergence behavior – inner iterations.

expected, unlike in UCDM, inner and outer iterations in PCHM start simultaneously, as shown in Fig. 19.

Based on Figs. 18 and 19, the convergence behavior of both approaches can be compared. As expected, the proposed PCHM model in conjunction with the cutting plane algorithm needs considerable less iterations than the UCDM to reach convergence.

6. Conclusions

This article presents a non linear homogenization model for piezoelectric composites polarized with interdigitated electrodes. The model can be considered as a generalization of an existing mechanical model for non linear mechanical composites. Starting from the pure constituents material properties and state, the model describes the composite electromechanical response. An existing phenomenological model for ferroelectric/piezoelectric materials is used for the piezoelectric fibers in this paper. Nevertheless, it could be stated that the modular design of the developed numerical tool allows to combine different pure constitutive models with the proposed homogenization model.

A relatively easy implementation within existing finite element codes represents, from the authors point of view, a substantial asset of the presented approach. All the numerical experiments carried out in the scope of this work have been performed with ABAQUS. Since ABAQUS does not support user defined materials with electric degrees of freedom, two user defined piezoelectric elements, namely a solid piezoelectric brick and a piezoelectric shell were used to host the proposed composite model.

The proposed composite model was tested by comparison with other numerical model, i.e a detailed model of the representative elementary volume. Comparisons of results obtained with both approaches are encouraging. The responses predicted by PCHM are in good agreement with the detailed FE/UCDM models analyzed. The proposed model presents a notably advantage regarding the computational efficiency. Moreover, the composite model is sensitive to well known composite constructive parameters. Additionally, the proposed model presents a notably advantage regarding the computational efficiency.

The application examples presented demonstrate the capabilities of the proposed model to be used as a design tool allowing to predict important technological issues such as operating range, linearity limits, non linear response and overall electromechanical coupling levels of devices using piezoelectric composites with interdigitated electrodes. These prediction capabilities are of great importance for the design of electromechanical systems that could be optimized and tuned up for a variety of working conditions.

Acknowledgments

The financial support of CONICET and the Research Council of National University of Tucumán (CIUNT) is gratefully acknowledged. The authors also wish to thank Amelia Campos for her collaboration in the English revision.

References

[1] Varadan VK, Vinoy KJ, Gopalakrishnan S. Smart material systems and MEMS: design and development methodologies. John Wiley and Sons, Ltd; 2006.
[2] Bhattacharya P, Suhail H, Sinha PK. Finite element analysis and distributed control of laminated composite shells using LQR/IMSC approach. Aerosp Sci Technol 2002;6:273–81.
[3] Choi S-C, Park J-S, Kim J-H. Vibration control of pre-twisted rotating composite thin-walled beams with piezoelectric fiber composites. J Sound Vib 2007;300:176–96.
[4] Guennam A, Luccioni BM. FE modeling of a closed box beam with piezoelectric fiber composite patches. Smart Mater Struct 2006;15:1605.
[5] Barbarino S, Bilgen O, Ajaj RM, Friswell MI, Inman DJ. A review of morphing aircraft. J Intell Mater Syst Struct 2011;22:823–77.
[6] Xu T-B, Siochi EJ, Kang JH, Zuo L, Zhou W, Tang X, et al. Energy harvesting using a pzt ceramic multilayer stack. Smart Mater Struct 2013;22:065015.
[7] Jang B. Advanced polymer composites: principles and applications. CRC Press; 1994.
[8] Maxwell J. A treatise on electricity and magnetism, Third ed., vol. 1. Oxford: Clarendon Press; 1891.
[9] Wagner K. Explanation of the dielectric behavior on the basis of the maxwell theory. Arch Electrotech 1914;2:371–87.
[10] Buesson W, Klinsberg C. Advanced polymer composites: principles and applications. Gordon and Breach Science Publishing, Inc.; 1963.
[11] Vel SS, Goupee AJ. Multiscale thermoelastic analysis of random heterogeneous materials: Part I: Microstructure characterization and homogenization of material properties. Comput Mater Sci 2010;48:22–38.
[12] Mori T, Tanaka K. Average stress in matrix and average elastic energy of materials with misfitting inclusions. Acta Metall 1973;21:571–4.
[13] Hill R. A self-consistent mechanics of composite materials. J Mech Phys Solids 1965;13:213–22.
[14] Benveniste Y. A new approach to the application of Mori–Tanaka's theory in composite materials. Mech Mater 1987;6:147–57.
[15] Bent A, Hagood N. Piezoelectric fiber composites with interdigitated electrodes. J Intell Mater Syst Struct 1997;8:903–19.
[16] Hashin Z. On elastic behaviour of fibre reinforced materials of arbitrary transverse phase geometry. J Mech Phys Solids 1965;13:119–34.
[17] Berger H, Kari S, Gabbert U, Rodriguez-Ramos R, Bravo-Castillero J, Guinovart-Diaz R, et al. Unit cell models of piezoelectric fiber composites for numerical and analytical calculation of effective properties. Smart Mater Struct 2006:451–8.
[18] Martinez M, Artemev A. Finite element analysis of broken fiber effects on the performance of active fiber composites. Compos Struct 2009;88:491–6.
[19] Deraemaeker A, Nasser H. Numerical evaluation of the equivalent properties of macro fiber composite (mfc) transducers using periodic homogenization. Int J Solids Struct 2010;47:3272–85.
[20] Wang B. Three-dimensional analysis of an ellipsoidal inclusion in a piezoelectric material. Int J Solids Struct 1992;29:293–308.
[21] Dunn M, Taya M. Micromechanics predictions of the effective electroelastic moduli of piezoelectric composites. Int J Solids Struct 1993;30:161–75.
[22] Chen T. An invariant treatment of interfacial discontinuities in piezoelectric media. Int J Eng Sci 1993;31:1062–72.

[23] Shodja H, Kargarnovin M, Hashemi R. Electroelastic fields in interacting piezoelectric inhomogeneities by the electromechanical equivalent inclusion method. Smart Mater Struct 2010;19:1–12.
[24] Odegard G. Constitutive modeling of piezoelectric polymer composites. Acta Mater 2004;52:5315–30.
[25] Dvorak G, Srinivas M. New estimates of overall properties of heterogeneous solids. J Mech Phys Solids 1999;47:899–920.
[26] Tan P, Tong L. Micromechanics models for non-linear behavior of piezoelectric fiber reinforced composite materials. Int J Solids Struct 2001;38:8999–9032.
[27] Aboudi J. Micromechanical analysis of fully coupled electro-magneto-thermoelastic multiphase composites. Smart Mater Struct 2001;10:867–77.
[28] Aboudi J. Hysteresis behavior of ferroelectric fiber composites. Smart Mater Struct 2005;14:726–45.
[29] Muliana AH. A micromechanical formulation for piezoelectric fiber composites with nonlinear and viscoelastic constituents. Acta Mater 2010;58:3332–44.
[30] Luccioni B. Constitutive model for fiber-reinforced composite laminates. J Appl Mech 2006;73:1–10.
[31] Jayendiran R, Arockiarajan A. Non-linear electromechanical response of 1–3 type piezocomposites. Int J Solids Struct 2013;50:2259–70.
[32] Lin C-H, Muliana A. Polarization switching responses of 1–3 and 0–3 active composites. Compos Struct 2014;116:535–51.
[33] Park J, Kim J. Analytical development of single crystal macro fiber composite actuators for active twist rotor blades. Smart Mater Struct 2005;14:745–53.
[34] Huber J, Fleck N. Multi-axial electrical switching of a ferroelectric: theory versus experiment. J Mech Phys Solids 2001;49:785–811.
[35] SIMULIA, ABAQUS Standard User's Manual V6.8, SIMULIA; 2008.
[36] Ben Atitallah H, Ounaies Z, Muliana A. A parametric study on flexible electroactive composites: importance of geometry and matrix properties. J Intell Mater Syst Struct 2014.
[37] Cocks A, McMeeking R. A phenomenological constitutive law for the behaviour of ferroelectric ceramics. Ferroelectrics 1999;228:219–28.
[38] Kamlah M, Tsakmakis C. Phenomenological modeling of the non-linear electromechanical coupling in ferroelectrics. Int J Solids Struct 1999;36:558–84.
[39] Landis C. Fully coupled, multi-axial, symmetric constitutive laws for polycrystalline ferroelectric ceramics. J Mech Phys Solids 2002;50:127–52.
[40] Semenov A, Liskowsky BH. Return mapping algorithms and consistent tangent operators in ferroelectroelasticity. Int J Numer Methods Eng 2009;81:1298–340.
[41] Landis C. Non-linear constitutive modeling for ferroelectrics. Curr Opin Solid State Mater Sci 2004;8:59–69.
[42] Lynch C. The effect of uniaxial stress on the electro-mechanical response of 8/65/35 PLZT. Acta Mater 1996;44:4137–48.
[43] Simo J, Hughes T. Computational inelasticity. Springer; 1998.
[44] Guennam A, Luccioni B. Piezoelectric shell FE for the static and dynamic analysis of piezoelectric fibre composite laminates. Smart Mater Struct 2009;18:095044 (12pp).
[45] Laskewitz B, Kamlah M. Finite element implementation of nonlinear constitutive models for piezoceramic materials. J Mech Mater Struct 2010;5:19–45.
[46] Schwaab H, Grünbichler H, Supancic P, Kamlah M. Macroscopical non-linear material model for ferroelectric materials inside a hybrid finite element formulation. Int J Solids Struct 2012;49:457–69.